Supporting Information

Manipulating the Water Dissociation Kinetics of Ni₃N Nanosheets via in-situ Interfacial Engineering

Shuwen Niu,[‡a] Yanyan Fang,[‡a] Jianbin Zhou,[‡a] Jinyan Cai,[a] Yipeng Zang,[a] Yishang Wu,[a] Jian Ye,[b] Yufang Xie,[a] Yun Liu,[a] Xusheng Zheng,[b] Wengang Qu,[*c] Xiaojing Liu,[*a] Gongming Wang[*a] and Yitai Qian[a]

a Hefei National Laboratory for Physical Science at the Microscale, Department of Chemistry, University of Science and Technology of China. Hefei, Anhui, 230026, P. R. China.

*Corresponding author. E-mail: wanggm@ustc.edu.cn, liuxj206@ustc.edu.cn.

b National Synchrotron Radiation Laboratory, University of Science and Technology of China. Hefei, Anhui, 230029, P. R. China.

c Xi'an Modern Chemistry Research Institute, Xi'an 710065, China.

*Corresponding author. Email: qwg1985@mail.ustc.edu.cn.

‡ These authors contributed equally to this work.

Experimental Section

The synthesis of Mo-NiO, Ni₃N, Mo-Ni₃N, Ni₃N/MoO₂ and Ni₃N/MoN.

The Mo-NiO nanosheets on nickel foams (NFs) were synthesized via a modified hydrothermal process.[1] First, Ni(NO₃)₂·6H₂O (1 mmol), NH₄F (1.8 mmol) and urea (4.4 mmol) were dissolved in 20 mL deionized water. And then, Na₂MoO₄·2H₂O (0.1 mmol) was added and stirred for 20 minutes. The as-prepared solution and a piece of NF were furtehr transferred to a 25 mL Teflon-lined stainless-steel autoclave and maintained at 120 °C for 6 h. After the autoclave cooled down naturally, the as-prepared resultant was collected and washed with deionized water and ethanol, respectively, and finally dried at 60 °C for 10 h. The obtained samples were finally annealed at 400 °C for 2 h with a heating rate of 10 °C per minute under the Ar atmosphere to obtain the Mo-NiO nanosheets. Ni₃N/MoO₂ nanosheets and Ni₃N/MoN on NF were prepared by annealing the Mo-NiO at 400 °C and 700 °C for 2h under NH₃ atmosphere, respectively. The Mo-Ni₃N was fabricated using the same procedure with a lower Na₂MoO₄·2H₂O amount (0.01 mmol), while the pure Ni₃N was synthesized without the addition of Na₂MoO₄·2H₂O.

Materials characterization.

X-ray powder diffraction (XRD, Philips, X'pert X-ray) was performed on a diffractometer of Cu Ka, λ=1.54182 Å. Scanning electron microscopy (SEM, JEOL-JSM-6700F, 5 kV of accelerating voltage) and transmission electron microscopy (TEM, Hitachi H7650, 100 kV of accelerating voltage) were employed to acquire the morphological and microstructural information. High resolution transmission electron microscopy (HRTEM), high angle annular dark-field scanning transmission electron microscopy (HAADF-STEM) and energy dispersive X-Ray spectroscopy (EDX) analysis were conducted on Talos F200X and JEMARM 200F microscope, respectively. The chemical states of the samples were measured by X-ray photoelectron spectroscopy (XPS) at the the BL10B end-station in the National Synchrotron Radiation Laboratory of Hefei, with the C1s (284.6 eV) as the calibration reference. X-ray absorption fine structure (XAFS) spectroscopy measurements were conducted at the beamline (BL14W1) of Shanghai National Synchrotron Radiation Facility (SSRF, China).

Electrochemical measurements.

The electrochemical measurements were carried out on the CHI760e electrochemical workstation in a typical three-electrode system, with Ag/AgCl (saturated KCl), graphite rod, the studied catalysts and 1.0 M KOH as the reference, counter, working electrodes and electrolyte, respectively. The polytetrafluoroethylene (PTFE) electrochemical cell was used for the electrochemical measurements, while the working electrodes were passivated by the insulating epoxy (Hardman Double Bubble HARDMAN, 04001) to avoid the capillary effect. The loading amounts for the Ni_3N, Ni_3N/MoO_2 and Ni_3N/MoN are ~1.5 mg cm^{-2}. The Pt/C catalyst ink was prepared by homogeneously dispersing 5 mg of the Pt/C (20 wt%) and 20 µL of 5 wt% Nafion solution in 1 mL water/ethanol (3:1 v/v) solution. Then, the catalyst ink was coated onto the NF with a Pt/C loading amount of 2 mg cm^{-2}. All potentials measured versus Ag/AgCl were calibrated to reversible hydrogen electrode (RHE) according to the Nernst equation: E (RHE) = E (Ag/AgCl) + 0.197 V + 0.059 pH. The polarization curves were obtained using linear sweep voltammetry (LSV) with a scan rate of 5 mV s^{-1}. The durability test was performed by chronopotentiometry technique with a fixed current density of 10 mA cm^{-2}. The electrochemical surface areas (ECSA) of the catalysts were estimated using the electrochemical double layer capacitance (C_{dl}).[2] To estimate the C_{dl}, cyclic voltammetry (CV) was carried out in the non-faradaic potential region from 0.228 to 0.328 V vs. RHE with various scan rates of 20, 40, 60, 80 and 100 mV s^{-1}, respectively. The capacitive current $\Delta j = (j_a - j_c)/2$ at 0.278 V is plotted versus the scan rate. Electrochemical impedance spectroscopy (EIS) measurements were performed at the overpotential of 50 mV with a potential perturbation of 5 mV amplitude in the range from 100 kHz to 0.01 Hz. TOF values were calculated using a previously reported method, in which the number of active sites was estimated as the amount of surface sites (including Ni, Mo, N and O atoms).[3] The geometrical areas for stability test is 1 cm^2. The Faradic efficiency for hydrogen production from 1.0 M KOH of Ni_3N/MoO_2 was evaluated in a H-type cell with an anion exchange membrane as the separator and 20 mL 1.0 M KOH as the electrolyte in each compartment, with a gas chromatography (HA GC-9560) for the hydrogen gas detection. The Faradic efficiency was calculated using the formula: Faradic efficiency = $2F*N_{H2}/Q = 2F*N_{H2}/(It)$, where F is the Faradic constant, I is the current, t is the running time and N_{H2} is the amount of H_2 production.

Density functional theory (DFT) calculations.

Plane-wave density functional theory (DFT) calculations were carried out using the CASTEP module in Materials Studio package of Accelrys Inc. The Perdew-Burke-Ernzerhof (PBE) functional of generalized gradient approximation (GGA) was used to evaluate the electron exchange-correlation energy.[4] The ultrasoft pseudopotentials were employed and the core electrons of atoms were treated using effective core potential (ECP). The kinetic energy cutoff was set to 500 eV for the plane-wave basis set. The Brillouin zone was sampled by a 3×3×1 Monkhorst-Pack mesh k-point sampling for structural optimization. DFT simulations were performed based on the crystal structures of hexagonal Ni_3N (a=4.616 Å, b=4.616 Å, c=4.298 Å, JCPDS No. 89-5144) with space group of P6322 and tetragonal MoO_2 with the space group of P42/mnm. The convergence tolerances for geometric optimization were set to 5.0 * 10^{-6} eV per atom for energy, 5.0 * 10^{-4} Å for maximum displacement, and 0.01 eV Å^{-1} for maximum force. The free energy changes (ΔG_H) for H* adsorption on Ni_3N (001) and MoO_2 (220) surfaces were calculated according to the equation: $\Delta G_H = E_{sur-H} - E_{sur} - E_{H_2/2} + \Delta E_{ZPE} - T\Delta S$,[5] where E_{sur-H} is the total energy of surface covered with a H, E_{sur} is the energy of clean surface, and E_{H_2} is the energy of H_2 in the gas phase, ΔE_{ZPE} is the zero-point energy change and ΔS is the entropy change. For this study, the value of $\Delta E_{ZPE}-T\Delta S$ on catalyst surface is 0.24 eV for H absorption.[5] H_2O absorption energy was calculated by the following equation, $\Delta E_{H_2O*} = E_{sur-H_2O*} - E_{sur} - E_{H_2O}$, where E_{sur-H_2O*} is the total energy of surface covered with a H_2O molecule, E_{H_2O} is the energy of a H_2O molecule in gas phase. A complete LST/QST approach was used to determine the transition state.
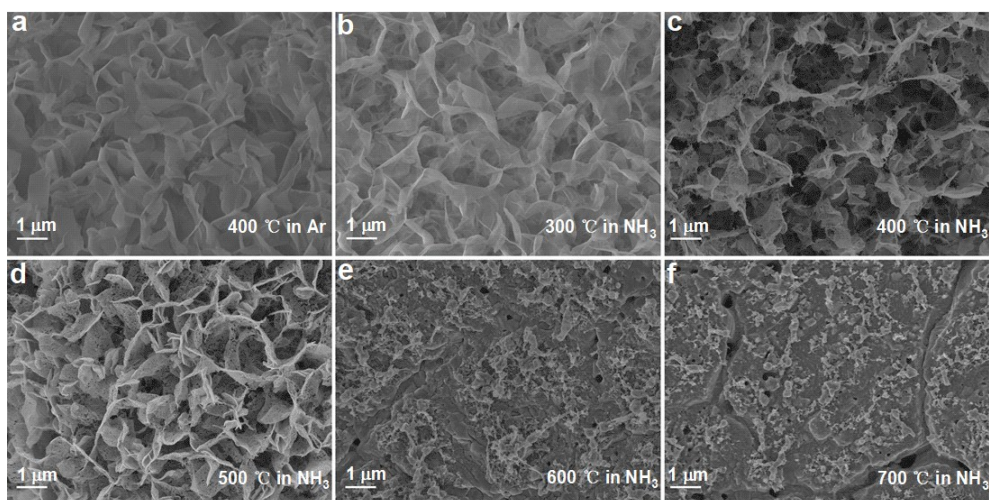
Fig. S1 SEM images of (a) Mo-NiO, and (b-f) Mo-NiO annealed at various temperatures in the range of 300-700 °C under NH$_3$ atmosphere, respectively.
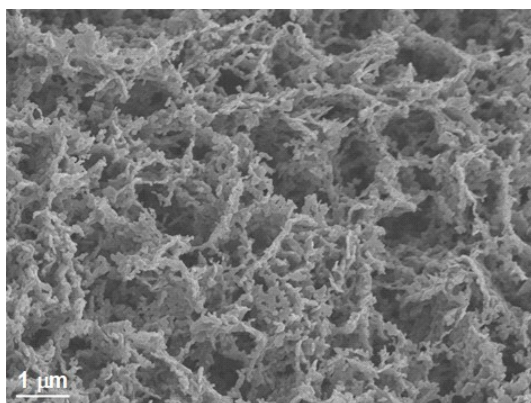
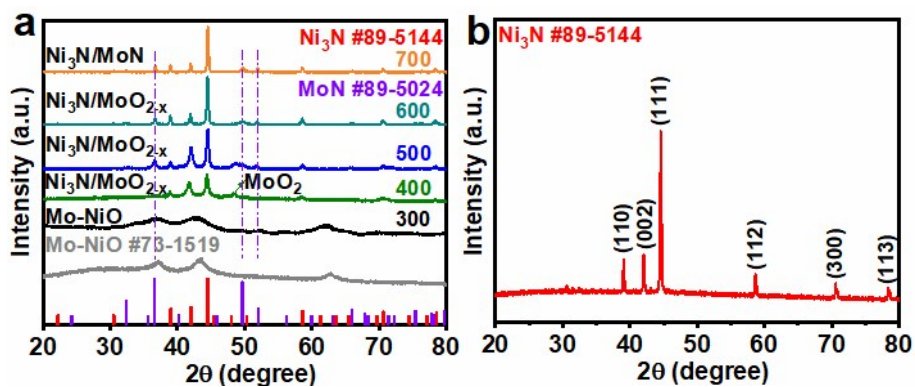**Fig. S2** SEM image of Ni$_3$N.

Fig. S3 (a) XRD patterns of Mo-NiO and Mo-NiO prepared at various temperatures. The dashed lines label the diffraction positions of MoN. (b) XRD pattern of pure Ni_3N.
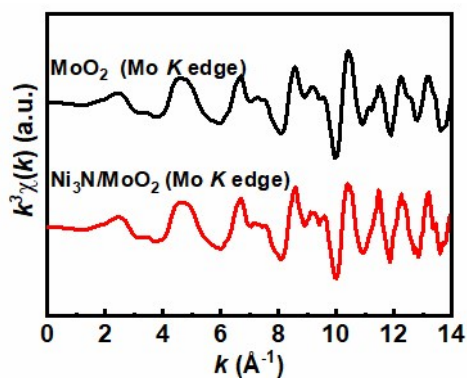

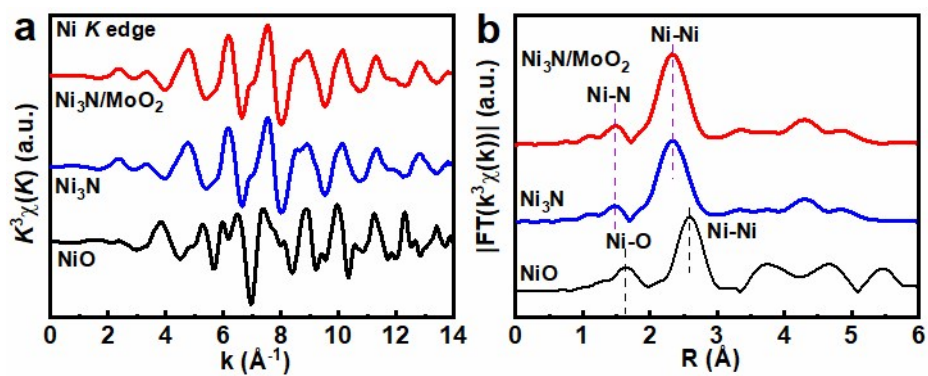**Fig. S4** (a) The Mo K edge EXAFS $k^3\chi(k)$ functions for MoO_2 and Ni_3N/MoO_2.

Fig. S5 (a) Ni K edge EXAFS $k^3\chi(k)$ functions for NiO, Ni_3N and Ni_3N/MoO_2 and (b) their Fourier transforms.
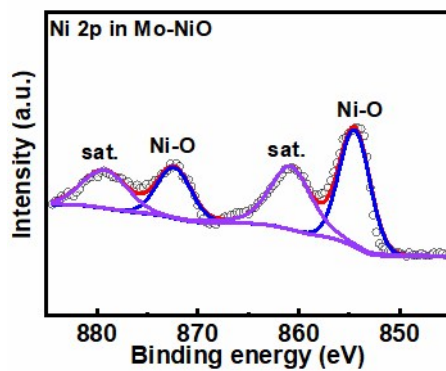

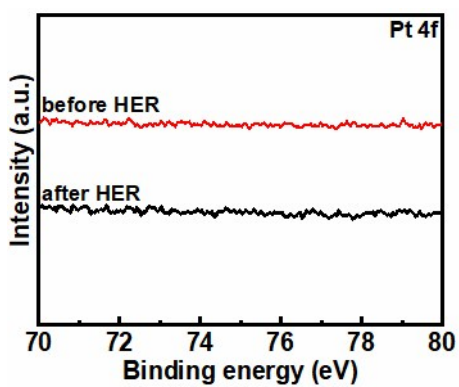**Fig. S6** XPS core-level spectrum of Ni 2p in Mo-NiO.

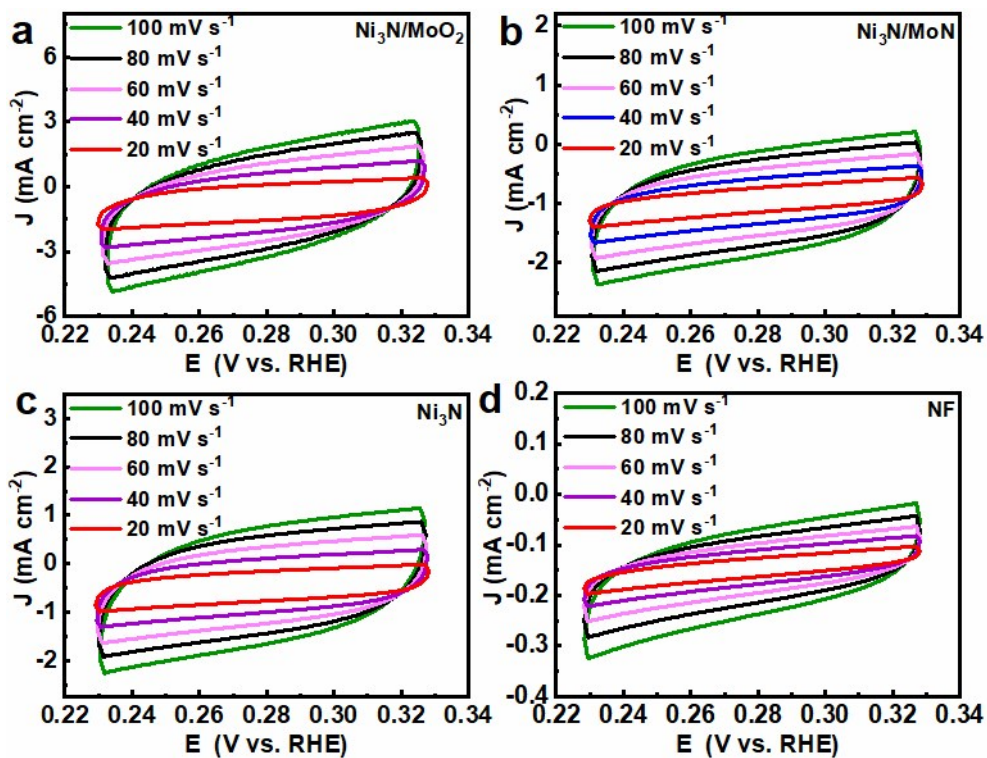**Fig. S7** The XPS Pt 4f spectra for the Ni_3N/MoO_2 before and after the HER stability test.

Fig. S8 CV curves of (a) Ni_3N/MoO_2, (b) Ni_3N/MoN (c) Ni_3N and (d) NF in the non-Faradaic range at the scan rates of 20, 40, 60, 80 and 100 mV s^{-1}, respectively.

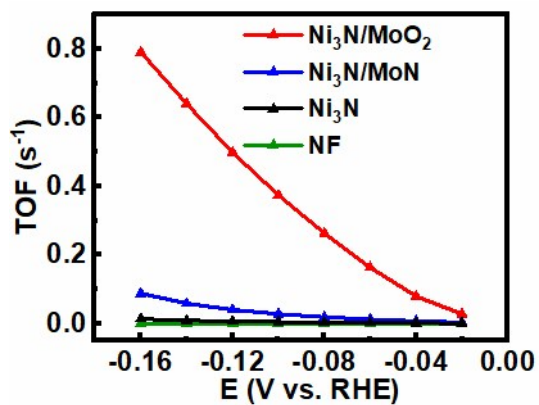**Fig. S9** Comparison of the TOFs of Ni_3N, Ni_3N/MoO_2, Ni_3N/MoN and NF at different potentials.
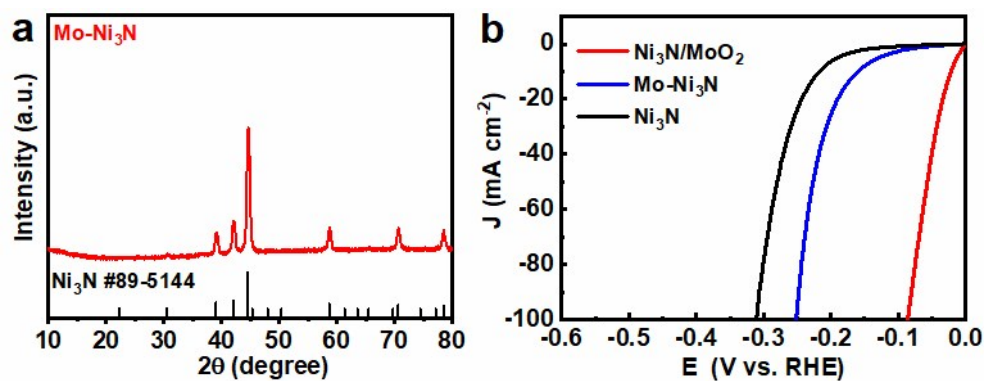
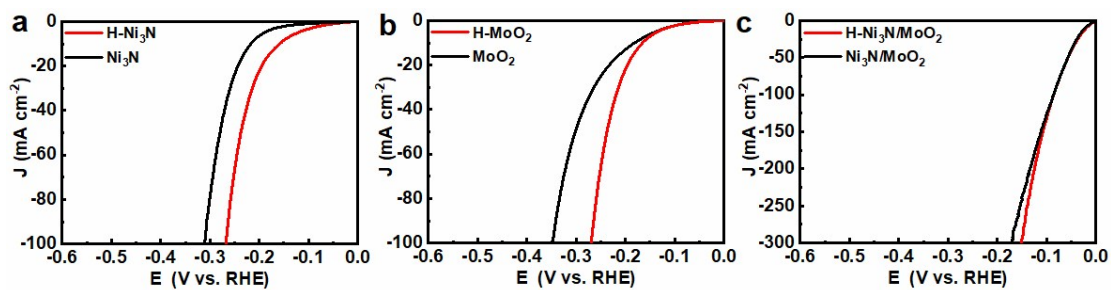**Fig. S10** (a) The XRD pattern of Mo-Ni$_3$N. (b) The polarization curve of Mo-Ni$_3$N compared with Ni$_3$N and Ni$_3$N/MoO$_2$.

Fig. S11 Polarization curves of (a) Ni$_3$N, (b) MoO$_2$ and (c) Ni$_3$N/MoO$_2$ and their hydrogen-treated counterparts.
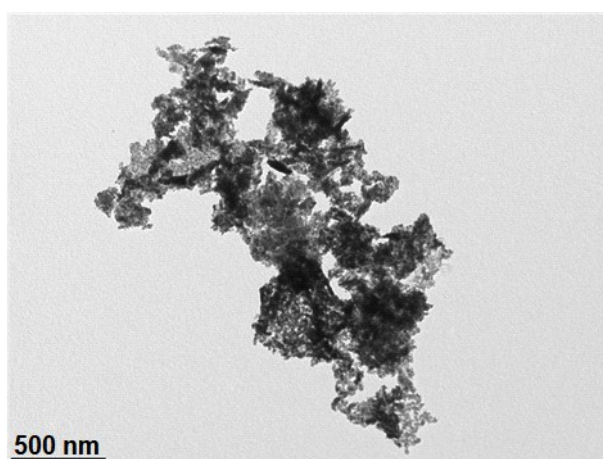

Fig. S12 TEM image of the Ni$_3$N/MoO$_2$ nanosheets after the HER stability test.
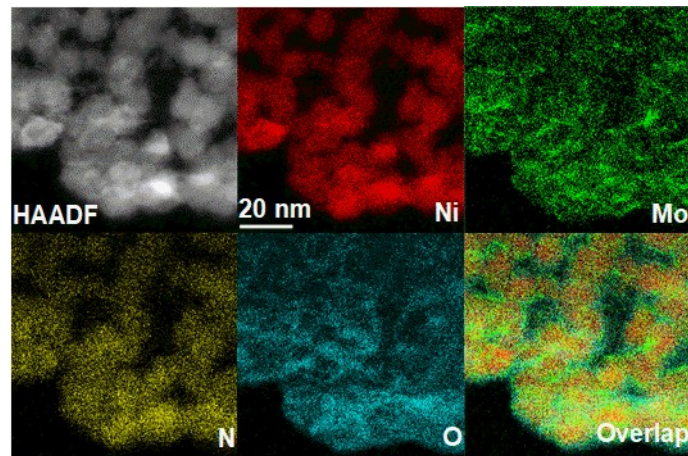
Fig. S13 HAADF-STEM element mapping images of the Ni$_3$N/MoO$_2$ nanosheets after the HER stability test.
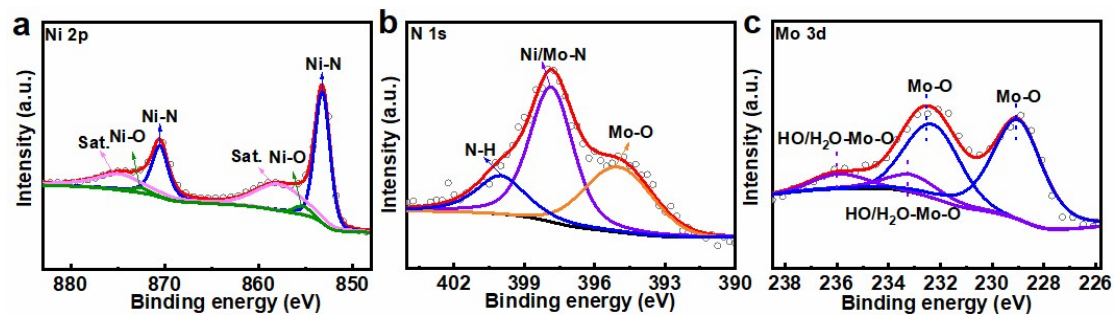
Fig. S14 XPS core-level (a) Ni 2p, (b) N 1s, (c) Mo 3d spectra of Ni$_3$N/MoO$_2$ after the HER stability test, respectively.
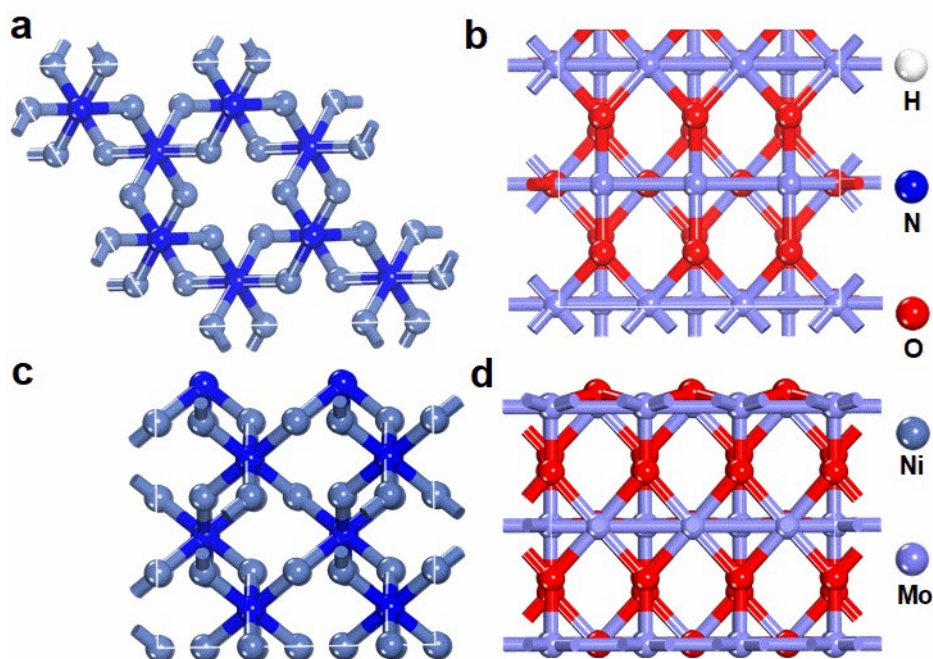
Fig. S15 The top-view and side-view structures of (a and c) Ni_3N and (b and d) MoO_2.
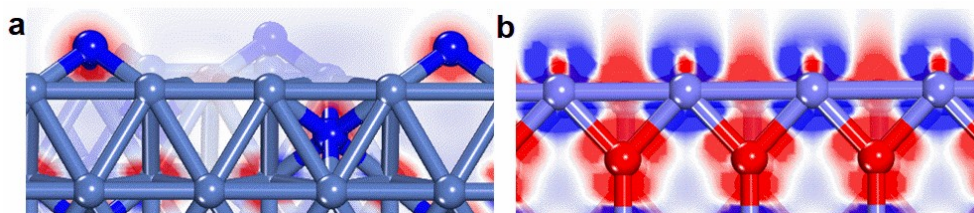
Fig. S16 The side-view slices of electron density difference images of (a) Ni_3N and (b) MoO_2 surfaces, respectively.
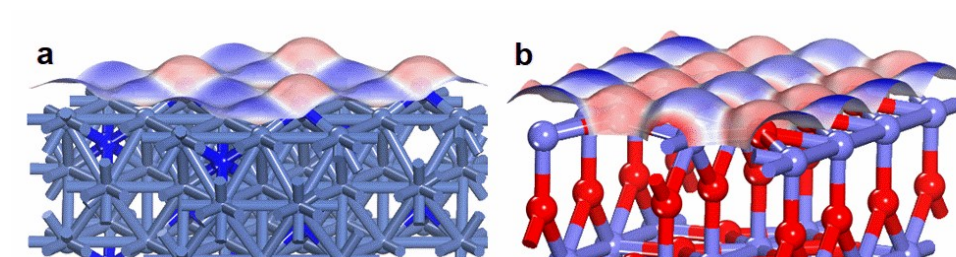
Fig. S17 The surface electrostatic potential maps based on the electron density difference of (a) Ni_3N and (b) MoO_2, respectively.

ΔG_{H^*}=0.6 eV ΔG_{H^*}=-0.01 eV

ΔG_{H^*}=-0.76 eV ΔG_{H^*}=-0.08 eV

Fig. S18 ΔG_{H^*} values of Ni_3N with the different N-Ni surfaces.

Table S1 The comparison of HER performances for Ni_3N/MoO_2 with the ever-reported metal nitrides electrocatalysts in alkaline medium.

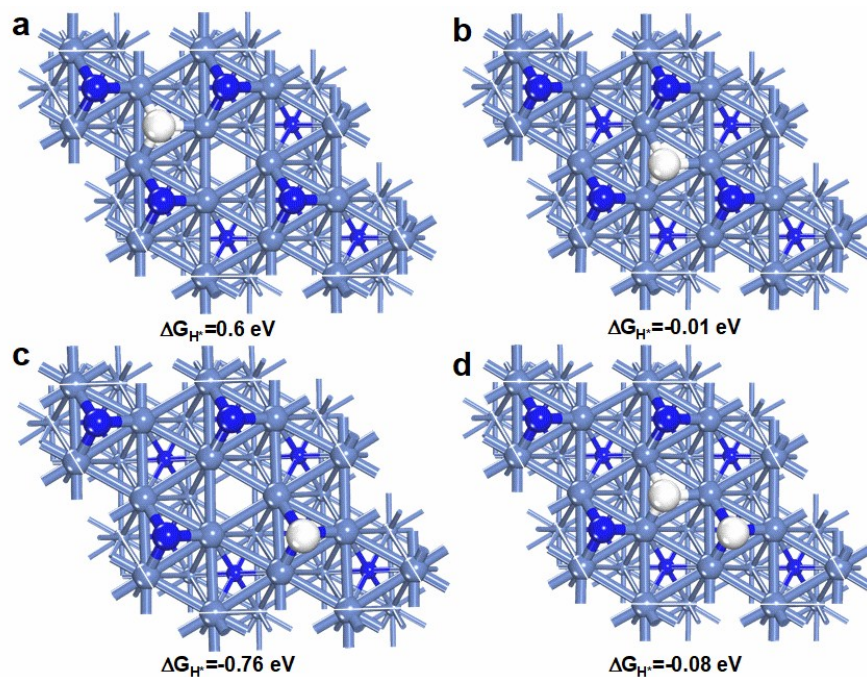| Catalysts	Morphologies	Substrate	η (mV) at 10 mA cm^{-2}	Tafel slopes (mV dec^{-1})	Electrolytes	Ref.
$Ni_3N/MoO_2/NF$	nanosheets	Ni foam	21 mV	46	1.0 M KOH	This work
Ni_3N	nanosheets	-	305 mV	-	1.0 M KOH	6
$Co-Ni_3N$	nanorods	carbon cloth	194 mV	156	1.0 M KOH	7
Ni_3FeN	nanoparticles	-	158 mV	42	1.0 M KOH	8
Fe_2Ni_2N	nanosheets	Ni foam	180 mV	101	1.0 M KOH	9
$Ni_3N/NiMoN$	nanosheets	carbon cloth	31 mV	64	1.0 M KOH	10
NiMoN	nanoparticles	-	24 mV	40	1.0 M KOH	11
NiMoN	nanoparticles	carbon cloth	109 mV	95	1.0 M KOH	12
TiN/Ni_3N	nanowires	titanium foil	21 mV	42	1.0 M KOH	13
Ni/WN	nanowires	carbon cloth	47 mV	71	1.0 M KOH	14
Co_3FeNx	nanowires	nickel foam	23 mV	94	1.0 M KOH	15
$V-Co_4N$	nanosheets	nickel foam	37 mV	44	1.0 M KOH	16
Ni_3FeN	nanoparticles	carbon cloth	238 mV	46	1.0 M KOH	17
Ni_3N_{1-x}	nanoparticles	Ni foam	55 mV	54	1.0 M KOH	18

References

1   Y. Q. Sun, K. X, Z. X. Wei, H. L. Li, T. Zhang, X. Y. Li, W. P. Cai, J. M. Ma, H. J. Fan and Y. Li, *Adv. Mater.*, 2018, **30**, 1802121.
2   C. C. McCrory, S. Jung, I. M. Ferrer, S. M. Chatman, J. C. Peters and T. F. Jaramillo, *J. Am. Chem. Soc.*, 2015, **137**, 4347-4357.
3   Y. S. Wu, X. J. Liu, D. D. Han, X. Y. Song, L. Shi, Y. Song, S. W. Niu, Y. F. Xie, J. Y. Cai, S. Y. Wu, J. Kang, J, B, Zhou, Z. Y. Chen, X. S. Zheng, X. H. Xiao and G. M. Wang, *Nat. Commun.*, 2018, **9**, 1425.
4   J. P. Perdew, K. Burke and M. Ernzerhof, *Phys. Rev. Lett.*, 1996, **77**, 3865-3868.
5   J. K. Nørskov, T. Bligaard, A. Logadottir, J. R. Kitchin, J. G. Chen, S. Pandelov and U. Stimming, *J. Electrochem. Soc.*, 2005, **152**, J23-J26.
6   D. Q. Gao, J. Y. Zhang, T. T. Wang, W. Xiao, K. Tao, D. S. Xue and J. Ding, *J. Mater. Chem. A*, 2016, **4**, 17363-17369.
7   C. R. Zhu, A. L. Wang, W. Xiao, D. L. Chao, X. Zhang, N. H. Tiep, S. Chen, J. N. Kang, X. Wang, J. Ding, J. Wang, H. Zhang and H, J, Fan, *Adv. Mater.*, 2018, **30**, 1705516.
8   X. D. Jia, Y. L. Zhao, G. B. Chen, L. Shang, R. Shi, X. F. Kang, G. I. N. Waterhouse, L. Z. Wu, C. H. Tung and T. R. Zhang, *Adv. Energy Mater.*, 2016, **6**, 1502585.
9   M. Jiang, Y. J. Li, Z. Y. Lu, X. M. Sun and X. Duan, *Inorg. Chem. Front.*, 2016, **3**, 630-634.
10 A. P. Wu, Y. Xie, H. Ma, C. G. Tian, Y. Gu, H. J. Yan, X. M. Zhang, G. Y. Yang and H. G. Fu, *Nano Energy*, 2018, **44**, 353-363.
11 T. Wang, X. J. Wang, Y. Liu, J. Zheng and X. G. Li, *Nano Energy*, 2016, **22**, 111-119.
12 Y. Q. Zhang, B. Ouyang, J. Xu, S. Chen, R. S. Rawat and H. J. Fan, *Adv. Energy Mater.*, 2016, **6**, 1600221.
13 Q. T. Zhang, Y. H. Wang, Y. C Wang, A. M. Al-Enizi, A. A. Elzatahry and G. F. Zheng, *J. Mater. Chem. A*, 2016, **4**, 5713-5718.
14 Z. C. Xing, D. W. Wang, Q. Li, A. M. Asiri and X. P. Sun, *Electrochim. Acta*, 2016, **210**, 729-733.
15 Y. Y. Wang, D. D. Liu, Z. J. Liu, C. Xie, J. Huo and S. Y. Wang, *Chem. Commun.*, 2016, **52**, 12614-12617.
16 Z. Y. Chen, Y. Song, J. Y. Cai, X. S. Zheng, D. D Han, Y. S. Wu, Y. P. Zang, S. W. Niu, Y. Liu, J. F. Zhu, X. J. Liu and G. M. Wang, *Angew. Chem., Int. Ed.*, 2018, **57**, 5076-5080.
17 Q. Chen, R. Wang, M. H. Yu, Y. X. Zeng, F. Q. Lu, X. J. Kuang and X. H. Lu, *Electrochim. Acta*, 2017, **247**, 666-673.
18 B. Liu, B. He, H. Q. Peng, Y. F. Zhao, J. Y. Cheng, J. Xia, J. H. Shen, T. W. Ng, X. M. Meng, C. S.Lee and W. J. Zhang, *Adv. Sci.*, 2018, **5**, 1800406.